

# Nanostructured OMO type Manganese Oxide – as Novel Support for Palladium towards Electrooxidation of Methanol and Ethylene Glycol

Ramanujam Kannan<sup>1,2</sup>, Kulandaivelu Karunakaran<sup>1</sup> and Samuel Vasanthkumar<sup>3,\*</sup>

<sup>1</sup>Department of Chemistry, Sona College of Technology, Salem – 636 005, INDIA.

<sup>2</sup>School of Nanosciences and Technology, Karunya University, Coimbatore – 641 114, INDIA.

<sup>3</sup>Department of Chemistry & Nanosciences and Technology, School of Science & Humanities, Karunya University, Coimbatore – 641 114, INDIA.

Received: January 31, 2012, Accepted: March 12, 2012, Available online: July 19, 2012

**Abstract:** Octahedral molecular sieve type manganese oxide (OMO) was synthesized by the ultra sonic assisted hydrothermal method, and was subsequently used as supportive material for palladium (Pd) metal towards the electrooxidation of methanol and ethylene glycol. The Pd nanoparticles were coated on the OMO by insitu reduction method. Low quantity of 5% Pd metal was used and the electrocatalytic activity was studied. The prepared OMO and the OMO/Pd nanocomposite were characterized by powder X-ray diffractogram (XRD), Scanning Electron Microscopy (SEM), Energy dispersive X-ray spectroscopy (EDS) and electrochemical methods. These studies demonstrated that the OMO can act as a good catalyst supporting material. The OMO helps to enhance the catalytic activity of Pd metal by supplying the active oxygen, which is extracted from the electrolytic solution. The electrooxidation of EG shows improved catalytic activity.

**Keywords:** Manganese oxide, Palladium, Electrooxidation, Fuel cell, Methanol oxidation

## 1. INTRODUCTION

Metal and Metal oxide nanoparticles have a large surface-area-to-volume ratio as compared to the bulk equivalents, making them particularly attractive candidates for catalytic applications. [1-5]. In the field of fuel cell research much attention has been paid for the preparation of metal catalyst in the nanoscale. In the electrooxidation of alcohols, Pd metal has been suggested for the acting as an effective anodic material. The poisoning of the active site of the catalyst is the major drawback in alcohol electrooxidation [1-3]. In order to reduce this poisonous effect various methods were adopted [1-17], such as placing a metal adjacent to the catalytic metal [1-5], alloys [15] or placing the catalyst on a suitable support [2,3, 12-14]. Recently, carbon nanotubes [6 12], carbon nanofibers [7,8], metal oxides etc. [9–12] have been used as supporting material for alcohol electrooxidation. Among these, metal oxides exhibit improved catalytic activity, because they readily donate oxygen atom to the catalyst, improving the catalytic activity [9-13].

Manganese oxides are one of the largest families of porous materials with various structures as found in manganese oxide minerals all over the world. Two major structures are important (1) Octahedral layer (OL) constructed of edge sharing  $\text{MnO}_6$  to form sheets with cations ( $\text{Na}^+$ ,  $\text{K}^+$ ) and in which water is present in between any two adjacent sheets and (2) octahedral molecular sieve (OMS) materials constructed by the edge and corner shared octahedral  $\text{MnO}_6$  [13,14 1,2].

Defects are very important in the application of OL and OMS materials. The main types of defect in OL and OMS materials are oxygen vacancies. The removal of an oxygen ion from OMS or OL materials can markedly influence conductivity. Oxygen vacancies can help as regards charge balance when doping is needed as long as an overall charge balance is fulfilled. Oxygen vacancies are also important in controlling conductivity. OMS materials retain number oxygen atoms in its structure [13]. By combining the active catalyst Pd on the OMS type manganese oxide material, the catalytic activity was expected to be enhanced. This nanocatalyst would act as a binary catalyst both the material would play the role for the electrocatalysis of the alcohol electrooxidation reaction.

\*To whom correspondence should be addressed: Email: kumar2359@yahoo.com

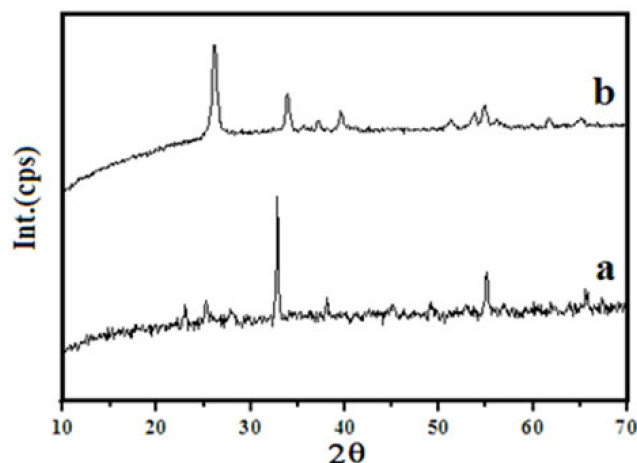


Figure 1. Power XRD patterns of the (a) OMO and (b) Pd/OMO nanocomposite.

In this study, OMO material was synthesized by simple ultrasonic assisted hydrothermal method and was used as a supportive material for Pd in the electrooxidation of methanol, and ethylene glycol in alkaline solution. The mechanism for the removal of intermediates was also discussed.

## 2. EXPERIMENTAL

### 2.1. Materials

Palladium acetate, ethylene glycol (Sigma–Aldrich), potassium permanganate, hydrogen peroxide (30% W/W), acetic acid, sodium acetate, potassium hydroxide, methanol, and ethylene glycol were received from Merck, India. All the chemicals were of analytical grade and were used without further purification.

### 2.2. Synthesis of OMO

Nanostructured OMO type manganese oxide material was synthesized by the hydrothermal method. In the typical synthesis, about 10 ml of hydrogen peroxide (10 % v/v) was added into the acetate buffer (equimixture of acetic acid and Sodium acetate) in 20 ml water. About 6.5 g  $\text{KMnO}_4$  was dissolved in 150 ml distilled water and the above mixture was added drop wise in to it with constant stirring. The whole reaction was performed in the ultrasonic bath. After the addition, the sonication was continued. After two hours the precipitate was separated by centrifugation (8000 RPM), washed several times with distilled water and dried using the domestic microwave oven. The prepared compound was characterized by powder XRD (Lab X 6000, Shimadzu), elemental analysis (EDS, INSTA FET, Oxford Instru.) and surface morphology (SEM, JSM 6390, JEOL). Particle size analysis (Zetasizer N 90).

### 2.3. Preparation of Pd coated OMO nanocomposite

The Pd modified OMO was synthesized by the *in situ* reduction method. In brief, appropriate quantity of 0.5 mM  $\text{Pd}(\text{ac})_2$  solution was taken in 5 ml ethanol; so as to achieve 5 % of Pd and 100 mg of OMO was added and stirred. After one hour, formaldehyde was added to the mixture drop wise and a reductive reaction was performed at room temperature. After six hours, the resulting product

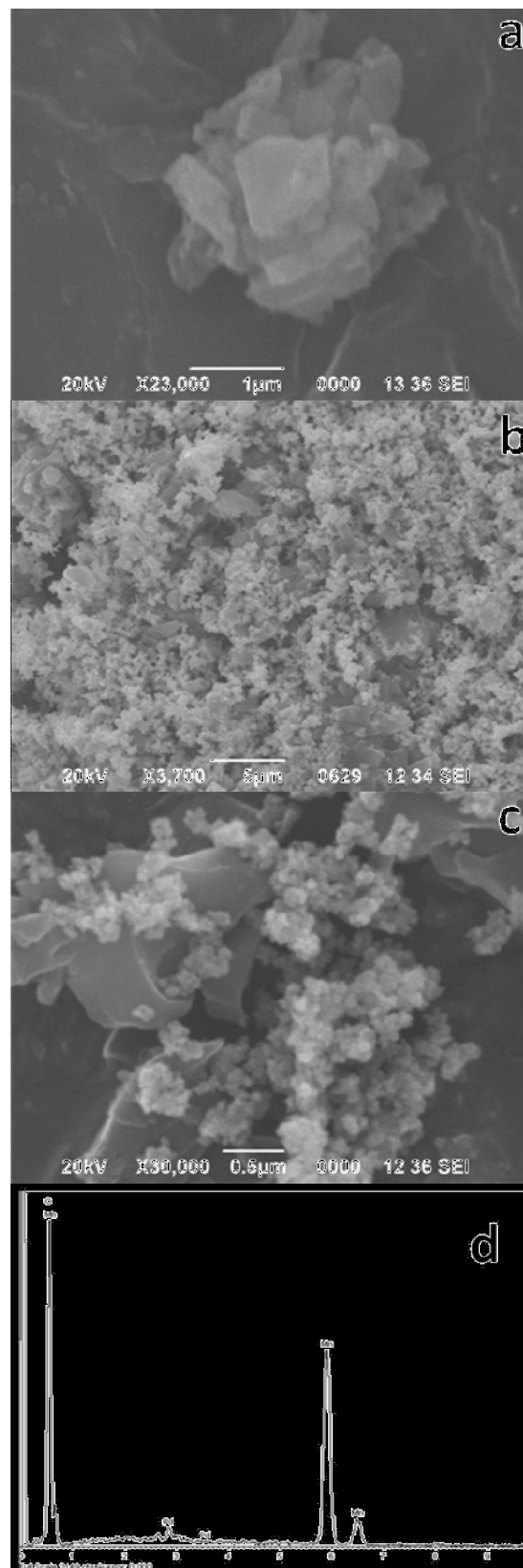


Figure 2. Scanning Electron Microscopic images of (a) OMO type Manganese oxide; (b & c) Pd metal coated OMO, (c) EDX spectrum for Pd/OMO.

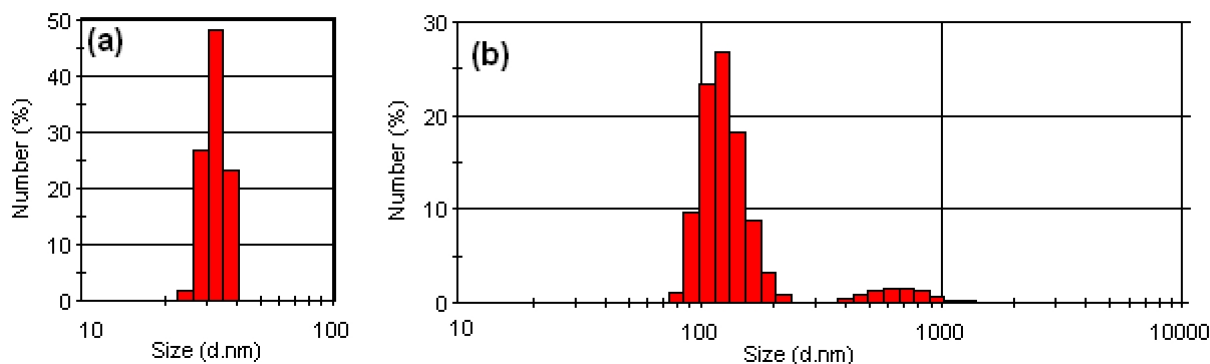


Figure 3. Particle size distribution of (a) OMO material and (b) OMO/Pd nanocomposite

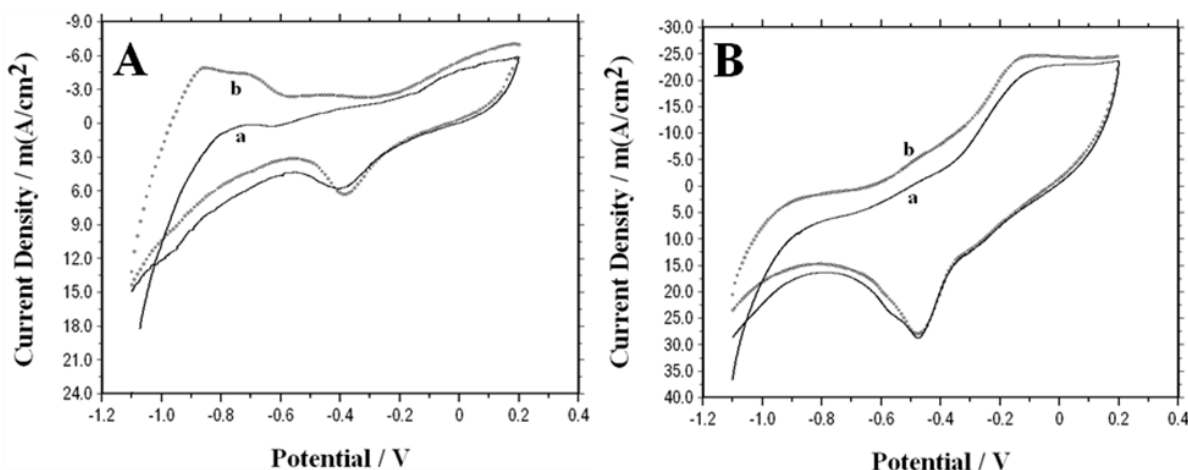


Figure 4. (A) Cyclic voltammograms of C/Pd and (B) OMO/Pd modified electrode at the (a) first and (b) fourth cycle in 1M KOH at 50mV/s

was filtered washed with distilled water, and then dried at 60 °C for 6 h.

#### 2.4. Preparation of OMO/Pd modified GC electrode

Electrochemical measurements were performed with a CHI660C electrochemical workstation (CH Instruments, USA) and a conventional three electrode cell equipped with computer controlled software. OMO/Pd nanocatalyst was ultrasonically dispersed in 0.5% of Nafion in ethanol solution. An aliquot of the OMO/Pd nanocatalyst/Nafion ink was dropped on the surface of the GC electrode and allowed to dry. The OMO/Pd nanocomposite catalyst modified GC electrode was the working electrode, a Pt wire served as the counter electrode and a Standard Calomel Electrode (SCE) was the reference electrode. For comparison, Pd supported on graphite powder and their electrodes were also prepared under the same preparative conditions.

### 3. RESULTS AND DISCUSSION

#### 3.1. Physical Characterizations of OMO and OMO/Pd catalyst

The crystal structure was analyzed by XRD (Fig.1), the prepared

OMO materials exhibits cryptomelane type OMS material (JCPDS #29-1020), and after the Pd medication the OMO peaks were masked by the Pd metal nanoparticles. This was confirmed by SEM studies. The surface morphology was tested by the Scanning Electron Microscopy. The SEM image reveals that the OMS material forms like a pedal or sheet like morphology. The Pd metal was covered uniformly on the OMO material and the higher magnification clearly shows the presence of Pd metal as smaller cubic nanoparticles on the OMO material (Fig.2 a-c). The chemical nature and the elements present were also tested by the EDS. The selective area analysis of elements present in the nanocomposite confirms the existence of Pd, Mn and O in the composite. The average percentage of Pd in the nanocomposite was 4.5%. The particle size of the prepared materials was analyzed by Diffused Reflectance Spectra – particle size analyzer, the OMS material shows about 32 nm and the Pd coated OMS material show about 180 nm even after one month. Hence, the present materials show excellent stability.

#### 3.2. Electrochemical behavior of OMO/Pd modified electrode

Fig.4a shows the first CV cycle recorded for C/Pd modified GC

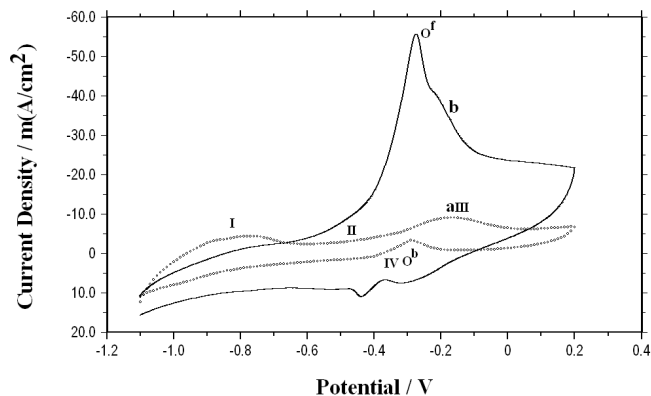


Figure 5. CVs of (a) Pd/OMO electrode in 1M KOH and electrooxidation of 1M CH<sub>3</sub>OH in (b) C/Pd and (c) OMO/Pd modified electrode in 1 M KOH [Scan rate 50 mV/s].

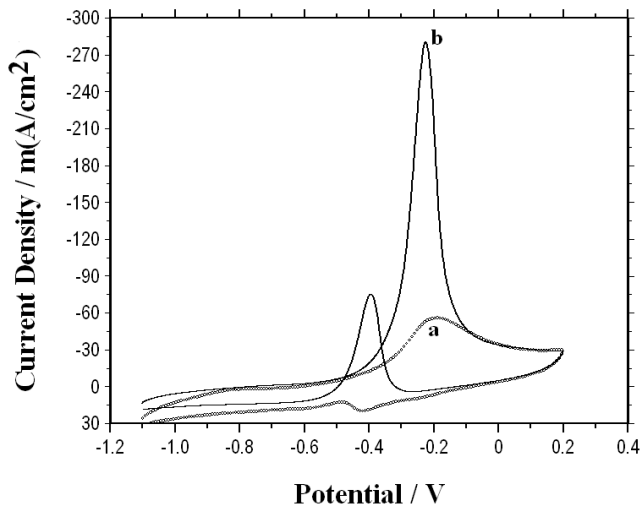


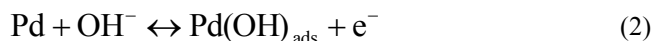
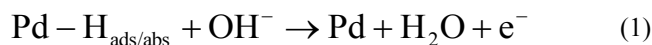
Figure 6. CVs of OMO/Pd modified electrode in 1M EG / 1M KOH (a) 4<sup>th</sup> and (c) 18<sup>th</sup> cycle [Scan rate 50 mV/s]

electrode in 1M KOH solution. During the first cycle, as soon as the forward scanning is started from  $-1.1$  V, the hydrogen absorption reaction starts at  $-0.8$  V occurs very gradually and reaches the maximum at  $-0.7$  V and stabilized at  $-0.6$  V. After  $-0.6$  V, the hydrogen desorption reaction occurs. The peak centered at  $-0.4$  V attributed to the reduction of PdO to Pd during the reverse scan. The hydrogen desorption rate is reduced when potential is taken to the negative region. On the increasing cycle, the rate increases further, on the fourth cycle, stable current density values are established. In the fourth cycle, the hydrogen adsorption rate increased drastically and hydrogen adsorption starts  $-0.8$  V, a slight shift in peak potential and peak current is observed in PdO reduction region is observed in the reverse scan. Fig.4b exhibits the CVs of OMO/Pd modified GC electrode in 1M KOH solution. In the first cycle, similar results like C/Pd are observed and the hydrogen absorption region was suppressed at OMO/Pd. In the fourth cycle, the hydrogen adsorption peak exhibits slight increased but compared to

the first cycle and enhanced peak current density was observed for OMO/Pd compared to C/Pd.

### 3.3. Electrochemical behavior of methanol and ethanol at OMO/Pd electrode

The prepared nanocatalyst OMO/Pd electrode was tested for the electrocatalytic activity for methanol oxidation. Pd has been deposited onto OMO nanoparticles as well as onto the fine graphite powder and the Methanol oxidation reaction (MOR) in 1M KOH / 1M CH<sub>3</sub>OH was compared (Fig.5). Fig. 5a shows the cyclic voltammogram of the C/Pd electrode in 1M KOH / 1M CH<sub>3</sub>OH solution. Three potential peaks can be observed during the positive-going sweep, which correspond to different electrochemical processes occurring on the surface of the Pd electrode. Peak I in the potential range between  $-0.9$  V and  $-0.7$  V is due to the oxidation of the absorbed and adsorbed hydrogen. Peak II is the adsorption of OH<sup>-</sup> on the Pd active site and the peak III, which emerges above  $-0.25$  V, can be attributed to the formation of palladium oxide (PdO).



In the MOR on the OMO/Pd electrode (Fig.5b), the hydrogen adsorption was significantly suppressed in the presence of methanol in the solution. The methanol oxidation started at  $-0.8$  V and the anodic peak O<sup>f</sup> occurs in the region of  $-0.6$  and  $-0.1$  V and the vertexes at (Ep)  $-0.278$  V. A less predominant backward oxidation peak at  $-0.38$  V was observed and which is comparatively less than C/Pd. In the hydrogen region, the suppression of peak can be attributed to the dissociative adsorption of methanol in the lower potential region.

In the MOR a relatively negative shift of oxidation peak potential and weaker backward oxidation peak compared to graphite (C/Pd) suggests that OMO material has a strong influence on electrocatalytic activity. The stability of the electrode was tested by increasing the cycling of the MOR upto 100 cycles in which the catalytic activity was almost same. Fig.5 indicates that the OMO/Pd nanocomposite has a better electrocatalytic activity than that of the C/Pd for the MOR, owing to the high surface area to volume ratio of OMO nanoparticles. This implies that OMO by itself is a good candidate for noble metal catalyst support. The reaction on the catalytic electrode was tested by varying the scan rate. The experimental results show that the electrode process was a surface controlled reaction.

In the EG electrooxidation, the formation of C<sub>2</sub> intermediates would affect the electrode activity and it is proposed that the “desorption – re-adsorption – further oxidation” plays an important role [15, 16]. Fig.6 shows the CVs for the EG oxidation at the fourth and the eighteenth cycle. In the forward scan, the scanning starts at  $-1.1$  V and exhibits a sharp peak for the EG electrooxidation at  $-0.23$  V and reaction complete and stabilize at  $+0.2$  V. In the reverse scan a prominent peak  $-0.42$  V for the oxidation intermediates formed during forward oxidation. The consecutive CVs shows

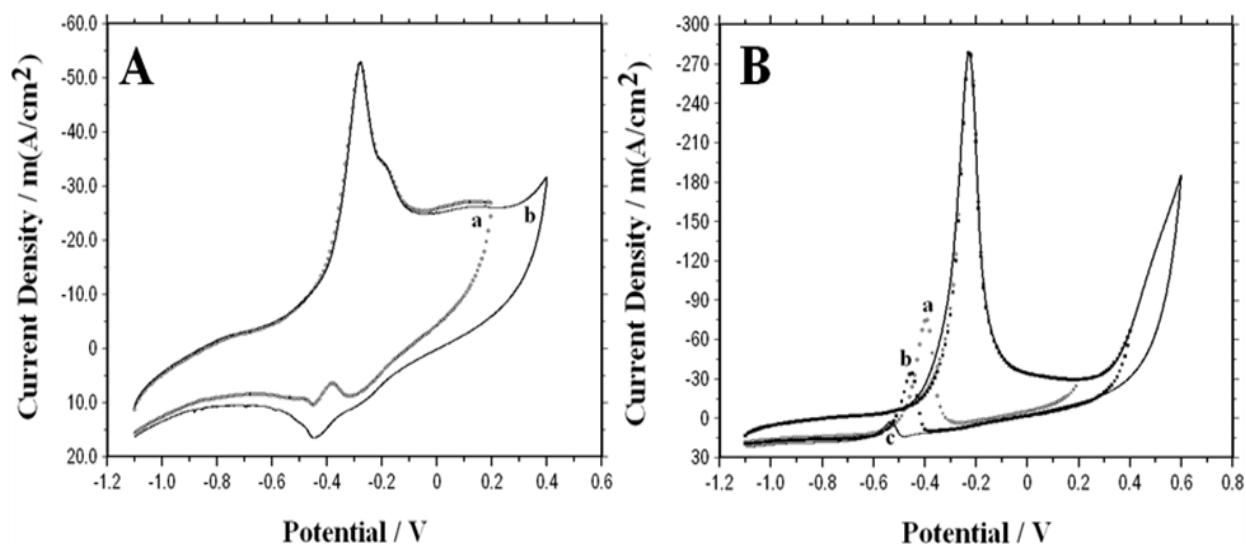
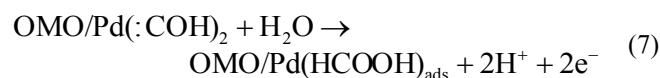


Figure 7. CVs of OMO/Pd modified electrooxidations of (A) methanol (1M CH<sub>3</sub>OH/ 1M KOH) in the scanning potential regions of (a) -1.1 to +0.2 , (b) -1.1 to +0.4 and (B) EG (1M EG / 1 M KOH) in the scanning potentials at (a) -1.1 to +0.2 , (b) -1.1 to +0.4 and (c) -1.1 to +0.6 V [scan rate 50 mV/s]

improved current response with increased number of cycles. This confirms the above information that the adsorption and re-adsorption of the C<sub>2</sub> intermediates on the OMO/Pd nanocomposite led to the further oxidation. Pure Pd metal suffers with the lower surface area. In the OMO/Pd nanocomposite in which the Pd metal attached to the OMO material resulting in an improved surface area. The presence of OMO would also help to oxidize the intermediates, leading to peak current increase and the maximum utilization of EG during the reaction.

The general reaction pathway of EG is given [15].

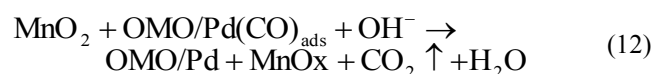
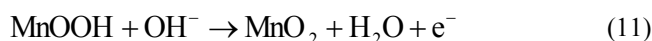


In the methanol and EG electrooxidation, the complete removal of CO/C<sub>2</sub> intermediates may not be possible, because it is strongly bonded with electrode (OMO/Pd) active sites. To oxidize these (CO/C<sub>2</sub>) intermediates require highly active oxygen. The availability of such active oxygen may not be possible in the potential window of -1.1 to +0.2 V, and it will be available at a potential of (> 0.2 V) at which the oxygen evolution reaction occurs leading to oxidation of the CO/C<sub>2</sub> intermediates.

The availability of the active oxygen is less in the lower potential

(E = +0.2 V), and by increasing the potential, the highly energetic oxygen is supplied by the OMO material, which helps to oxidize the poisonous intermediate. The active oxygen atom was extracted from the electrolytic solution by the OMO material by the reversible redox process [17].

Fig.7a shows the CVs of OMO/Pd electrode in 1M KOH / 1M CH<sub>3</sub>OH in the range of (a) -1.1 V to +0.2 V, (b) -1.1 V to +0.4 V. In the two CVs the anodic oxidation peak (O<sup>I</sup>) occurs in the region -0.6 V to -0.1 V with the vertex potential of -0.278 V (E<sub>p</sub>). A minor backward oxidation peak Ob<sup>I</sup>, with E<sub>p</sub> = -0.38 V occurs in the CV whose scanning potential up to +0.2 V and this was completely eliminated by increasing the scanning potential up to +0.4 V. This suggests that the CO intermediates adsorbed on the electrode surface were completely removed. Fig.7b exhibits the CV cycles of OMO/Pd nanocomposite catalyst modified electrode in 1 M KOH / 1 M EG in the potential range of (a) -1.1 V to +0.2 V, (b) -1.1 V to +0.4 V, (c) -1.1 V to +0.6V. In all the CVs the anodic oxidation peak (O<sup>I</sup>) occurs in the region -0.45 V to -0.1 V with the vertex potential of -0.23 V (E<sub>p</sub>). A prominent backward oxidation peak Ob<sup>I</sup>, with E<sub>p</sub> = -0.42 V occurs in the CV whose scanning potential up to +0.2 V. A relatively weaker backward oxidation peak was observed for the scanning potential up to +0.4 V and +0.6 V.



The favorable electrooxidation of poisonous intermediated formed during the course of methanol and EG of CO/C<sub>2</sub> is derived from supplying the active oxygen by the support material. In the

electrooxidation the backward oxidation current was very minimum for methanol which is because of the active oxygen being extracted from the electrolyte by the manganese oxide material through a reversible redox process. The proposed reaction scheme explains the same. By simply increasing the potential, the active oxygen atom would be extracted from the electrolyte and this will oxidize the intermediates effectively. In these reactions, the supporting material would supply and help to extract the active oxygen from electrolyte [17].

#### 4. CONCLUSION

Octahedral molecular sieve type manganese oxide was tested as supporting material for Pd towards electrooxidation of methanol and ethylene glycol. The experimental results showed that improved electrocatalytic activity of the nanocatalyst (OMO/Pd) towards methanol and ethylene glycol electrooxidation. The oxidation potential was shifted to a lower potential and the peak current was also increased. By increasing the scanning potential the poisonous intermediates were completely removed by oxidation. The maximum oxidation current density of 280 mA for 1M KOH / 1M EG was observed. The OMO acts as an excellent supportive material, which extracts the active oxygen from the electrolyte and oxidizes the intermediate.

#### 5. ACKNOWLEDGEMENT

The authors thank the DST, India for provided the research facilities under DST nanomission project. The authors express gratitude to the authorities of Karunya University, Coimbatore, and Sona College of Technology, Salem, for their kind support.

#### REFERENCES

- [1] Z. Qi, H. Geng, X. Wang, C. Zhao, H. Ji, H.C. Zhang, J. Hu, Z. Zhang, *J. Power Sources*, 196, 5823 (2011).
- [2] J.B. Goodenough, A. Hamnett, B.J. Kennedy, R. Manoharan, S.A. Weeks, *J. Electroanal. Chem.*, 240, 133 (1988).
- [3] J.B. Goodenough, A. Hamnett, B.J. Kennedy, S.A. Weeks, *Electrochim. Acta*, 32, 1233 (1987).
- [4] B.E. Conway *Electrodes of Conductive Metallic Oxides*, Part A, S. Trasatti (Ed.), ELSEVIER, Amsterdam, 1981.
- [5] M. Shibata, S. Motoo, *J. Electroanal. Chem.*, 209, 151 (1986).
- [6] Y. Zhao, X. Jang, J. Tian, F. Wang, L. Zhan, *Int. J. Hydrogen Energy*, 35, 3249 (2010).
- [7] Z. Liu, X. Zhang, L. Hong, *Electrochem. Commun.*, 11, 925 (2009).
- [8] T. Maiyalagan, K. Scott, *J. Power Sources*, 195, 5246 (2010).
- [9] C. Xu, Z. Tian, P. Shen, S.P. Jiang, *Electrochim. Acta*, 53, 2610 (2008).
- [10] Y.C. Wei, C.W. Liu, W.D. Kang, C.M. Lai, L.D. Tsai, K.W. Wang, *J. Electroanal. Chem.*, 660, 64 (2011).
- [11] R. Kannan, K. Karunakaran, S. Vasanthkumar, *Appl. Nanosci* DOI 10.1007/s13204-011-0049-5.
- [12] R. Kannan, K. Karunakaran, S. Vasanthkumar, *Ionics*, (Accepted for publication).
- [13] S.L. Suib and J. Mater. Chem., 18, 1623 (2008).
- [14] Q. Feng, H. Kanoh and K. Ooi, *J. Mater. Chem.*, 9, 319 (1999).
- [15] A. Serov, C. Kwak, *Appl. Catal. B: Environ*, 97, 1 (2010).
- [16] Z. Jusys, J. Kasier, R.J. Behm, *Langmuir*, 19, 6759 (2003).
- [17] S. Mohammed, E. Deab, *J. Adv Res*, 3, 65 (2012).